Research Article

Journal of Applied Material Science & Engineering Research

Effect of Ti and B on the Wartensitic Transformations and Microstructures in Polycrystalline Cu-12(wt. %) Al-4(wt. %) Ni High Temperature Shape Memory Alloys

Shahadat Hussain[1,2], Abhishek Pandey[2], Ashish Kumar Jain[2] and Rupa Dasgupta[1, 2*]

[1]*Academy of Scientific and Innovative Research, CSIR-Advanced Materials and Processes Research Institute, Bhopal, M.P. 462026 India*

[2]*Smart and Functional Materials, CSIR-Advanced Materials and Processes Research Institute, Bhopal, M.P. 462026, India*

[*]Corresponding author

Rupa Dasgupta, Academy of Scientific and Innovative Research, CSIR-Advanced Materials and Processes Research Institute, Bhopal, M.P. 462026 India, Tel: +91 755-245827; Fax: +91 755-2457042; E-mail: dasguptarupa@gmail.com

Submitted: 17 Jan 2018; **Accepted**: 23 Jan 2018; **Published**: 17 Feb 2018

Abstract

Addition of grain refiners/alloying elements is one of the most effective methods to reduce the grain size in the alloys, thereby, enhancing the mechanical and other properties of the alloy. Titanium and boron are added to polycrystalline Cu-12Al-4Ni (wt. %) high temperature shape memory alloy in the present study which were synthesized using induction melting furnace in air atmosphere. The alloys were betatized for one hour at temperature of 920°C and then were quenched in iced water. Further, they were characterized using the techniques of optical microscopy, X ray diffractometry, differential scanning calorimetry and hardness testing. Boron added alloys show thick plates of β_1' martensite with increase in transformation temperature as compared to base alloy whereas titanium added alloys show mixture of fine and thick plates of β_1' as well as γ_1' martensite with decrease in the transformation temperature as compared to the base alloy. Precipitation of second phase takes place in both titanium and boron alloying to Cu-Al-Ni base alloys.

Keywords: Shape Memory Alloys, Phase Transformation, Optical metallography, X ray diffraction, Martensite

Introduction

Shape Memory Alloys (SMAs) are smart materials with the ability of remembering its shape after deformation. They can recover their original shape after plastic deformation subjected to the application of heat or magnetic field. These materials undergo crystallographic reversible transformation betweenmartensite to austenite phase and exert enough recovery stress to regain their original shape before deformation [1]. Martensitic transformation is a first order shear dominated diffusion less transformation. This is a solid to solid state transformation in which marten site phase nucleate and grows from the parent phase of austenite after martensitic starttemperature (Ms). This phase transformation from martensite phase to austenite phase is termed as reverse transformation whereas phase transformation from austenite to martensite is termed as forward phase transformation. The temperature, at which reversible martensitic to austenitic phase transformation occurs, is termed as transformation temperature or transition temperature and is a characteristic feature of SMAs. During phase transformation in SMA, it undergoes martensitic transformation from high symmetry austenite phase (usually bcc) to low symmetry martensite phase (usually monoclinic or orthorhombic). Both the phases, namely, martensitic phase as well as austenitic phase coexist during the phase transformation. Several variants of martensitic phase are formed during the phase transformation from austenite to martensite, owing to the fact that austenite phase has higher symmetry than that of martensite phase.

These materials have huge potential to be used in diverse fields of applications such as automotive sectors, aerospace sectors, mini actuator and micro-electromechanical systems (MEMS), robotics and biomedical fields [2-6]. Thermo-responsive shape memory alloys are one which responds to heat. NiTi and copper based SMAs are most important alloy systems which show thermo-responsive shape memory behaviors and have attracted extensive research works. NiTi SMAs have excellent shape memory properties and transformation ductility and therefore they have been successfully used commercially in all different fields mentioned above but they have some drawbacks such as high cost, manufacturing difficulties, moderate fatigue characteristics and low transition temperatures which limits its applications.

Among copper based SMAs, three alloy systems are very popular: Cu-Al-Ni, Cu-Al-Mn and Cu-Zn-Al. Among these three alloy systems, Cu-Al-Ni alloy shows better thermal stability, high super elastic effect, high damping coefficient and small thermal hysteresis as compared to other two. This makes Cu-Al-Ni alloys suitable for high temperature applications. In order to use these alloys commercially for high temperature applications extensive research

works are being carried out throughout the globe. But these alloys have some drawbacks too which limit their commercial success. Brittleness, intergranular fractures, low recovery strain, martensite stabilization, low fatigue and low bandwidth [7,8]. These alloys are generally manufactured using casting routes which have some inherent problems such as loss of materials, impurities pick up, oxidation and improper mixing of constituents which deteriorate the properties of the alloys. Cu-Al-Ni SMAs are very much prone to intergranular fractures owing to several reasons such as grain coarsening during solidification, large grain size of 1 mm and large elastic anisotropy cause stress concentration at the grain boundaries, presence of impurities such as Bi, Sb, S, P, O and Pb among which Bi and Sb are highly deleterious, formation of α, NiAl andγ_2 (Cu_9Al_4) phaseat the grain boundaries also cause embrittlement and segregation of metalloids at the grain boundaries [9,10].

In order to solve above problems many approaches were used such as change in synthesis methods and parameters (for examples: replacing conventional casting route with induction melting, arc melting with vacuum or inert atmosphere attachments and continuous casting such as melt spin, rapid solidifying etc.), variations in thermal cycles and processing, ultra-rapid quenching, grain boundary engineering such as precipitation of an FCC solid solution second phase along the grain boundaries have been found effective method to improve ductility,different mechanical deformations, alloying of elements to the base alloys and grain refiners [11]. Many researchers have suggested grain refining and alloying as a potential method to inhibit the grain growth during high temperature treatments and reduce the grain size during solidification [12]. Alloying elements are used to reduce grain sizes so as to avoid intergranular fractures, inhibit martensite stabilization, modify the phase diagrams, adjust the transformation temperatures, improve the workability of the alloys and enhance the service life of SMA devices.The quantity of alloying materials is optimized for the desired results in the main alloy system. Very small addition of grain refiners may not serve the purpose since small quantity of alloying may not be sufficient enough to control the grain growth during annealing or may not be able to reduce grain sizes during solidification. On the other hand, large quantity of grain refiners may change the chemical compositions of main alloy system, thus hampering the designed properties and behavior of the original alloy system and may cause precipitation of undesirable second phase [13,14]. Majority of researchers have suggested the practice of micro alloying with the fourth elements to obtain fine grain size [15-21]. B, Vand Zrare used as grain refiners for Cu-Zn-Al alloys while Fe, B, Ti,Cr, nanoCeO_2, and Gdhave been used for Cu-Al-Ni alloys [12,13,18-28].

Prerequisite for exhibiting shape memory effect is the presence of single β phase as a high temperature phase. In Cu-Al-Ni alloy, this single β phase is obtained if the composition of Al lies between 10-14 wt.% and that of Ni lies between 2-4wt.% in the alloy system [1,29]. There occurs ordering reactions of β phase at the high temperature: from disordered β with bcc structure to β_2 of B_2 structures to ordered parent phase β_1 of DO_3 cubic superlattice structures.

$$\beta\ (A2) \longrightarrow \beta_2\ (B2) \longrightarrow \beta_1\ (DO_3)$$

On equilibrium cooling, α, NiAl and γ2 phases are formed, while during quenching with high cooling rate, four types of martensite form namely α1'(6R), β1' (18R1),β1''(18R_2) and γ_1'(2H) where R represents rhombohedral and H represents hexagonal structures;depending on chemical composition, test temperature, mode of load applications and crystal orientation [30-32]. In order to obtain higher transformation temperature in case of Cu-Al-Ni SMAs, the quantity of Al should be decreased but the minimum accepted level of Al is 10 wt% [33].Cu-Al-Ni alloys with 10 wt% Al can never be betatized fully, therefore their structures will always be biphasic consisting of α(FCC) + β1 (DO_3) [34]. With low aluminum content 6R martensitic phases are dominant whereas at high aluminum content, 2H martensite phases are dominant phases in the quenched alloys while in between ranges of Al both the mixture of β_1' as well as γ_1' phases are present since β_1'' martensite phases are very rare. In order to obtain sufficiently high transformation temperatures (150-200°C), Al contents should be lower than 14wt % but with this composition; formation of γ_2 phase is inevitable unless alloying of other element are done such as to be able to extend the single β_1 phase region and to lower the electron/atom ratio [30,35]. Transformation temperatures are highly sensitive to the chemical compositions of the alloys. Slight variation in the transformation temperatures cause drastic change in the transformation temperatures of the SMAs which hamper its shape memory properties. Therefore, very close control on the composition of the alloy synthesized should be kept in order to obtain desirable transformation temperature. Loss of volatile matters and low melting elements such as Al, Zn etc. should be consider during the synthesis of alloys so that final materials may have desired composition which subsequently influence the shape memory properties and transformation temperatures of the SMAs.

Titanium as alloying element/grain refiner is most effective additive to Cu-Al-Ni SMAs. It has been found that addition of titanium results into grain refining, reduction of grain coarsening at high temperature treatment of the alloy, entrapping segregated oxygen at the grain boundaries so as to prevent intergranular fractures and improves the mechanical properties of the alloy [13,25,36,37]. Addition of Ti leads to precipitation of second phase in the matrix of the alloy which is known as X-phase. Some researchers have determined the crystal of these X-phases in Ti added alloys and reported two types of X-phase particles: one is X_L and other is X_S with different sizes, shapes and coherency factor with the matrices [38].Moreover, anotherhas reported four types of X-phases and their origin of formation depending on the composition of alloys, quenching rate, quenching temperature, betatizing temperatures and way of cooling and ageing treatment [39].

Boron as alloying element/grain refiner has been used by some researchers in Cu-Al-Ni-Mn alloys with different thermal cycles showing the increase in martensitic transformation temperatures [40]. Morris observed that addition of boron led to precipitation of boride particles of small and large sizes and found that ductility of Cu-Al-Ni SMAs increased due to these boride particles precipitated after boron addition to Cu-Al-Ni alloy along with Mn addition [9]. He also reported that boron addition lowered the degree of order in the alloys. It has also been reported that addition of boron along with manganese increases the ductility of the Cu-Al-Ni SMAs as well as increases the yield strength and tensile strength at the room temperature [41].

To the knowledge of authors, very few works have been done in boron alloying to Cu-Al-Ni SMAs without the additional alloying of Mn to it. Therefore in this paper, an attempt has been made to study the effect of boron addition to Cu-Al-Ni shape memory alloy without any additional alloying of Mn to it. Effect of Ti addition is also being

investigated in the paper in terms of microstructures, transformation temperature and hardness in order to establish a comparative study among the base alloy, boron and titanium added alloys.

Materials and Methods

Figure 1 shows the schematic representation of the experimental procedures adopted during the study. The Cu-12Al-4Ni (wt%)-X (=Ti and B) alloys were synthesized through induction melting of raw materials in elemental form with the purity of 99.9%.One kilogram of raw materials were taken in graphite crucible and were heated to the temperature more than 1300°C till complete melting took place. Melting was carried out in open air and during the melting process mixing of the components of alloys were ensured by stirring through mechanical stirrer using hand. Thereafter, hot molten metal was poured in preheated graphite die. Castings in form of rectangular plates of thickness 3 mm were obtained after solidification. Six alloys namely CAN (base alloy), CANB1, CANB2, CANT1, CANT2 and CANT3 were casted. Addition of 0.1wt% of boron was done in CANB1 alloy, 0.3wt% of boron in CANB2 whereas addition of 0.1 wt% Ti, 0.3wt% Ti and 0.5wt% Ti were done in CANT1, CANT2 and CANT3 respectively. After solidification, the ingots were sectioned using grinder in different shapes and sizes for different characterization processes.

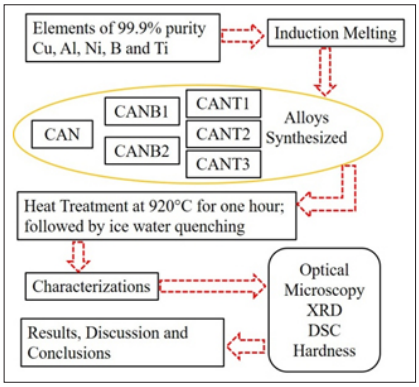

Figure1: Flowchart showing scheme of study

The alloys were heat treated in a muffle furnace for one hour at the temperature of 920°C followed by quenching in an ice water bath. The heat treated alloys were further processed in term of shape and size for different characterization processes in order to study their characteristics using characterization techniques of optical microscopy, differential scanning calorimetry, XRD and hardness testing.

The samples were prepared through standard metallography processes and etched in the solution of 5 mL ferric chloride, 25 mL hydrochloric acid and 100 mL water at room temperature. Grinding and polishing of the samples were carried out using automatic grinder and polisher of Buehler make, model EcoMet 3000. Diamond suspension solution was used for fine polishing with varying sizes of 9µm, 3µm up to 1µm.

Optical micrographs were imaged with an LEICA microscope equipped with an METALLOPLAN model, a digital USB camera, and Leica Application Suite version 3.6.0 software. The micrographs were taken at room temperature with different magnification in order to study the shape, size and morphologies of grains and second phase precipitates with their distribution and orientation in the grain as well as along the grain boundaries.

The phases obtained in the quenched samples were confirmed using the XRD techniques with peak matching method using JCPDS data. X-ray diffraction of the quenched samples were carried out with the aid of X Ray Diffractrometer (Bruker Make; Model D8 Advanced). The samples were made to undergo the 2theta rotation from 10°to 90°at room temperature at the scanning rate of 0.01°/sec using Cu Kα target. K_β peaks stripping and noise reduction were carried out before the analysis of the peaks obtained.

Differential Scanning Calorimetry of all samples, weighing less than 40 mg (in form of small chips obtained either through drilling or shaping) were carried out by the means of apower compensated differential scanning calorimter (Make: Mettler Toledo, Model:DSC1STARe SYSTEM, sensitivity: <1 µW, temperature accuracy: 0.1K and enthalpy accuracy: generally <1%). The device was calibrated using the standards of Bi, In, Sn and Zn. The samples were analyzed using the heating and cooling rate of 10°C/min in forward and reverse cycle from room temperature to 600°C under the protective atmosphere of nitrogen gas. The rate of nitrogen gas supply was 20 mL/min. STARe Evaluation software was used to calculate the different thermodynamic parameters associated with the phase transformation during heating as well as cooling scan of the quenched alloys.

Hardness Testing of the quenched samples were carried out using Vickers scale of hardness under 5 Kgf load for 10 seconds at room temperature. The hardness tester (KB 250 BVRZ, Pruftechnik, Germany) with diamond indenter of right pyramid with a square base and an angle of 136 degrees between opposite faces were used. Three readings for each samples were obtained; which were averaged to calculate their mean hardness value. Hardness testing was carried out on the well grinded and polished surface of the alloys.

Chemical composition of as-cast alloys was determined using optical emissive spectroscopy technique with the help of spectrometer (Bruker Make; Model Q4 TASMAN). Sparkis generated with the polished surface of the alloy in a protective environment of argon gas.

Results and Discussion

Thermal Analysis

Figure 2 and Figure 3 shows the DSC thermograms of the quenched alloys. These curves have been obtained during the cooling scan run. Out of six alloys, four of them show distinct transformation peaks and other two with addition of 0.1 wt% of boron (CANB1) and titanium (CANT1) did not show any distinct phase transformation peaks in the DSC Thermogram.Martensitic start and Martensitic finish temperatures have been marked in the figure as Ms and Mf respectively. In Figure 2 it can be observed that addition of boron [Figure 2(c)] had led to shift in the transformation peak toward the right as compared to that of alloy CAN in Figure 2(a). In Figure 3(b) and Figure 3(c), it can be observed that addition of titanium has shifted the transformation peaks toward the left as compared to that of CAN.

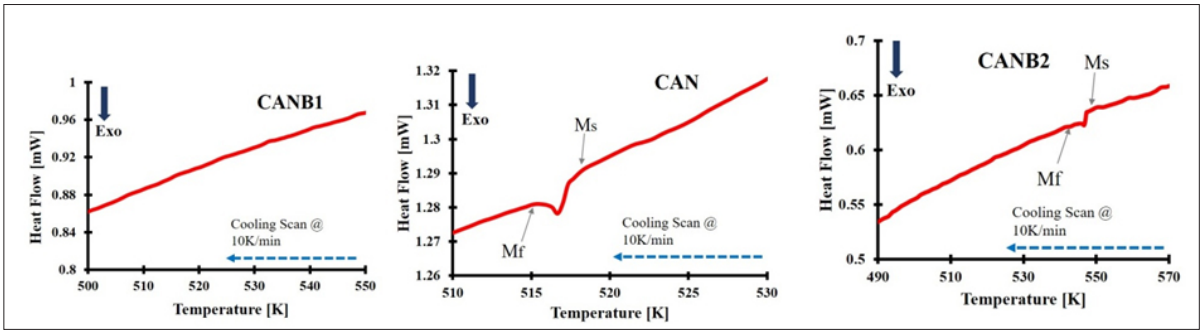

Figure 2: DSC Plots of Quenched Base Alloy and B added Alloys (a) CAN Alloy (b) CANB1 Alloy (c) CANB2 Alloy

Cu-Al-Ni based SMAs are very sensitive to their compositional change. Very slight changes in the compositions of the alloys result into drastic change in their transformation temperatures. Alloying leads to the change in the chemical compositions as well as formation of some insoluble precipitates, which subsequently cause increase or decrease in the transformation temperature of these alloys. Martensitic transformation temperature of Cu-Al-Ni SMAs are related by the following equation [42].

Ms (°C) = 2020 - 134(wt% Al) - 45(wt%Ni)……(i)
The general relationship between the martensitic transformation temperature and chemical composition of the alloys are given by following relation
Ms = D + ∑ eiEi…..(ii)
Where D = constant, Ei = amount of element, ei = constant corresponding to appropriate quantity of elements.

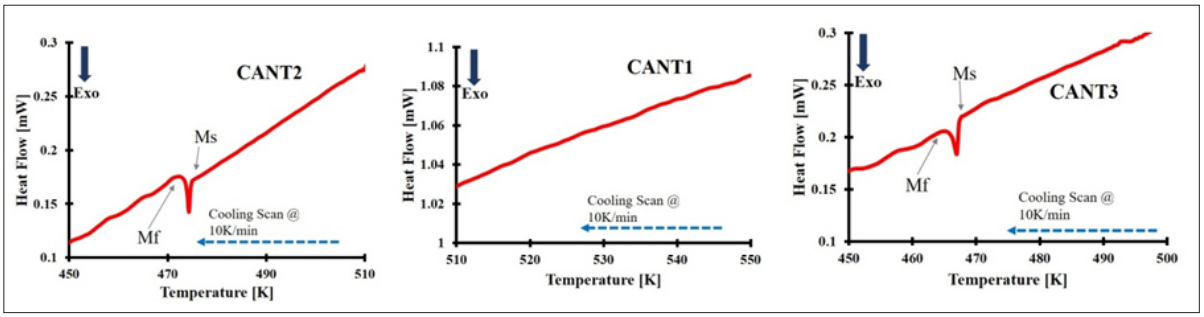

Figure 3: DSC Plots of Quenched Ti added Alloys (a) CANT1 Alloy (b) CANT2 Alloy (c) CANT3Alloy

Alloy Composition	M_s (K)	M*f* (K)	Al (wt %)	Ni (wt %)	Grain Refiner (wt %)
CAN	517	515	12.15	3.98	—
CANB1	—	—	11.00	3.99	0.1
CANB2	547	544	10.65	4.0	0.3
CANT1	—	—	10.69	3.90	0.1
CANT2	475	471	10.95	3.91	0.3
CANT3	467	463	10.81	4.08	0.5

Table1: Transformation Temperature and Chemical Composition

Table 1 shows the chemical compositions and forward transformation temperatures of the quenched alloys. It can be observed that the transformation temperatures of all the four quenched alloys are greater than 373K (100°C) which makes them suitable for high temperature applications. Ms and Mf temperature of all four alloys are listed in the Table 1. Applying the first equation [equation (i)] for martensite start temperature for CAN alloy, the transformation temperature comes near about in the range of obtained result. But all the four alloys show deviations in their transformation temperatures from that of the calculation based on above equation. This deviation can be explained in following ways.

Transformation temperatures of the Cu-Al-Ni based SMAs are highly sensitive to the chemical compositions and the cooling rates during quenching [15]. Thermal cycling changes the degree of order owing to the fact that thermal cycling induces thermal stress in the material and introduces dislocations in the alloy, thereby changing the transformation temperature. During quenching with different cooling rates, variations in the content of Al may take place within solution in the matrix due to formation of γ_2 phase which will surely affect the transformation temperature of the alloy.

In addition, addition of grain refiners leads to precipitation of second phases which deplete the concentration of Al and Ni from matrix and consequently transformation temperature of the alloys change. In this present work the experimentally obtained transformation temperatures are the combined effects of grain refinement, compositions, solid solution hardening and precipitation of second phases.

Phase Analysis

Phase analysis with the aid of X ray diffraction studies reveals the formation of γ_1'phases, β_1'phases and X-phases in the quenched samples. Predominantly there is β_1'phase with 18R structures in all six quenched alloys. There are seven diffraction planes which have been identified in the XRD plots shown in Figure 3, out of which planes (122), (0018), (128), (2010) and (040) are identified with β_1'phase which have self accommodating structures responsible for the shape memory effect in these alloys.

In CAN alloy only γ_1'and β_1'martensitic structures are found. Planes (200) shows the diffraction plane of γ_1' phase with 2H structureswhich is found in the quenched samples of

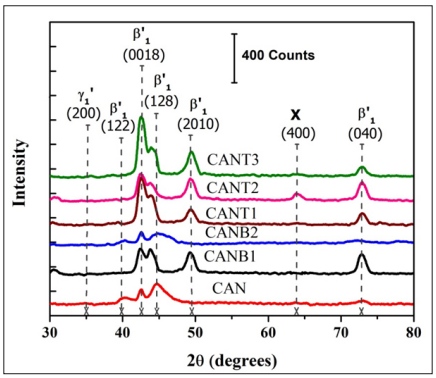

Figure 4: XRD Plots of Quenched Alloys

CAN, CANT1, CANT2 and CANT3, though the intensity peak of this phase is not very sharp and high. Plane (400) corresponds to the X phase formation in CANT2 and CANT3 alloys. Formation of X-phase has taken place in the alloy CANT1 also, but its peak is not visible in the XRD plots. X-phase has cubic Heusler type superstructure of DO3 structure which further ordered into L21 structure. Both DO_3 and $L2_1$ have almost similar structures. Researchers have calculated the crystal structures of X-phases using the XRD data and microscopic results [38]. There is no peak in CAN, CANB1 and CANB2 which corresponds to the diffraction from plane (400), as it can be confirmed from the microstructures that there is no X-phase formation in the alloys other than Ti added alloys.

Peaks corresponding to Plane (2010) and (040) are distinct in CANB1, CANT1, CANT2 and CANT3 whereas peak corresponding to diffraction plane (128) shift toward left in CANB1, CANT1, CANT2 and CANT3 whereas it becomes a little wide in CANB2. Crystal structure of β1' is reported to be orthorhombic in case of Cu-Al-Ni SMAs [25].

Microstructures

The optical micrographs of all six alloys show the formation of martensitic phases. There are two types of martensite which are formed in these quenched alloys. These two variants of martensite are β_1'with 18R structures and γ_1'with 2H structures. Predominately β_1'martensite phases in these alloys have self accommodating structures. CAN alloy shows different orientation of martensite plates in different directions with varying thickness of martensite plates. γ_1' phase can be identified in the right bottom corner of the micrograph in Figure 5(a). γ_1'phase has lamella structure with parallel plate plates oriented in vertical direction in the micrograph. There is no such distinct precipitation of second phases in CAN alloy which can be observed in the optical micrograph.

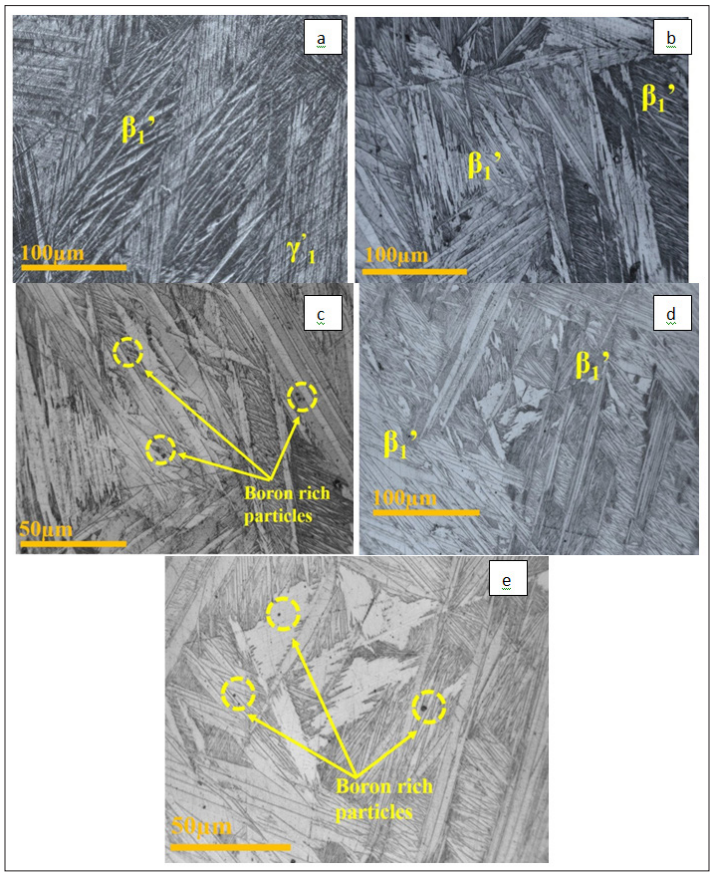

Figure 5: Optical Micrographs of Quenched Base Alloy and B added Alloys
(a) CAN Alloy
(b) CANB1 Alloy
(c) CANB1 Alloy Showing Boron Rich Particles
(d) CANB2 Alloy
(e) CANB2 Alloy Showing Boron Rich Particles

Figure 5(b) shows the microstructure of alloy after boron addition of 0.1 wt%, i.e., CANB1. Figure 5(c) show the precipitation of second phase in the CANB1 alloy with higher magnification. Morrisand Font et al. have confirmed these precipitations as the boron rich particles [9,40,41]. It can be observed that only β_1'variant of martensite phase is formed. These martensite phases have lower degree of order [9]. The thickness of martensite plates has decreased and they are oriented in different directions. The length of martensite plates is predominately smaller than that of CAN alloy but some large sizes of martensite plates are also observed. The growth of large martensite plate is hindered by the intersecting plates of small and finer martensite plates. On the careful examination of micrographs in the Figure 5 (c), two types of black dots can be found in the micrograph. These black dots represent the precipitation of second phase on addition of boron to CAN alloy. One of them is found at the grain boundaries and other one can be found in the martensite plates. Along the grain boundaries, these are mainly boron rich precipitates with aluminum in higher concentration as compared to matrix as confirmed by other researchers [9,40].

These are aluminum boride particles which are homogeneously distributed in the alloy. These particles influence the mechanical properties by hindering the movement of microtwins within the

martensite band. There are size variationsin these particles. Some of them are very small while some of them are big enough to be observed clearly in the optical micrograph. Some researchers have suggested that these small particles may be the undissolved boron during the casting [40]. These particles rich in boron having different scattering factor compared with that of the other component of the alloy, are visible in the micrograph with different contrast as compared to that of the matrix.They do not interact with the martensite twins as suggested by some studies [9,40].

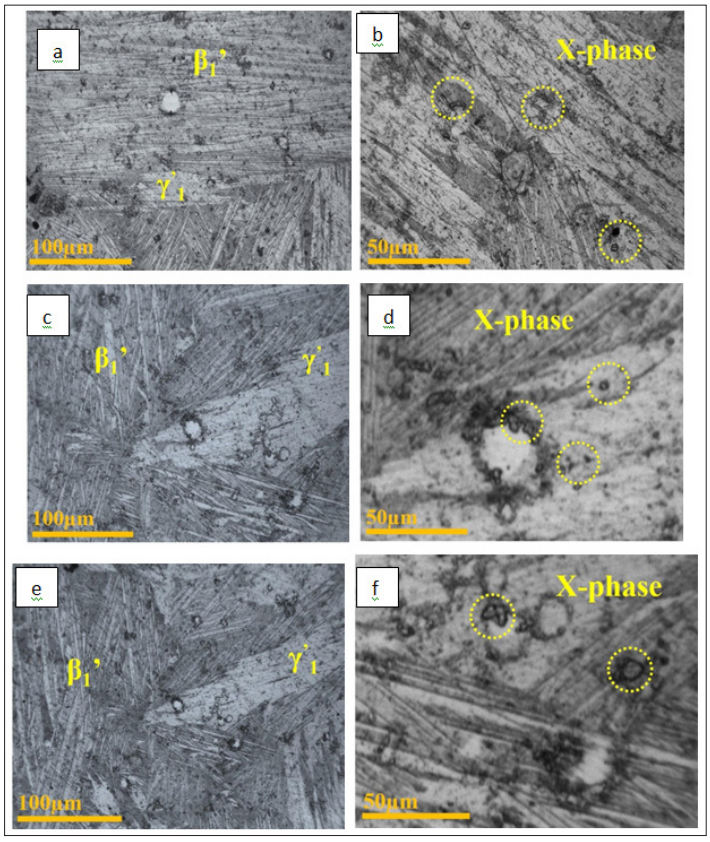

Figure 6: Optical Micrographs of Quenched Ti added Alloys
(a) CANT1 Alloy
(b) CANT1 Alloy Showing X-phase
(c) CANT2 Alloy
(d) CANT2 Alloy Showing X-phase
(e) CANT3 Alloy
(f) CANT3 Alloy Showing X-phase

Figure 5(d) and (e) shows the microstructure of 0.3 wt% boron added alloys, i.e., CANB2 and the precipitation of second phase in CANB2 respectively. It can be observed that number of coarse and thick plates have decreased as compared to that with CANB1, which are replaced by thinner and smaller plates. In Figure 5 (e), it can be observed that second phase precipitation has taken place similar to that of Figure 5 (c). There are two size variation of these second phases and researchers have identified these phases as boron rich precipitates [9,40,41,43].

They have confirmed the presence of aluminum boride as well as boron particles in the alloys with boron addition. These second phase particles affect the mechanical as well as the thermal characteristics of the alloy. Due to increase in the concentration of boron, some of the 18R phases have disappeared in the XRD analysis such as the peaks corresponding to the planes of (2010) and (040) are absent in CANB2 whereas the peak corresponding to the plane (128) has shifted right of that of CANB1 with less intensity. Martensite plates in CANB1 alloy [Figure 5 (b)] are very sharp with distinct sharp edges while in CANB2 [Figure 5(c)], martensite plates are blunt and twinned structures show smooth edges as observed in the optical micrographs.

Figure 6 (a-f) shows the microstructures of alloys after addition of titanium. Figure 6 (a) shows the microstructure of alloy CANT1 in which 0.1 wt% Ti addition has been made while Figure 6 (b) shows the precipitation of second phase after Ti addition in CANT1 alloy at higher magnification. Similarly Figure 6 (c) shows the microstructure of CANT2 alloy with their corresponding precipitation of second phase in Figure 6 (d) whereas Figure 6 (e) shows the microstructure of CANT3 alloy with their corresponding second phase precipitation termed as X-phase in all the cases of Ti addition at higher magnification in Figure 6 (f). It can be observed that predominately β_1' variant of martensite has been formed in these quenched alloys whereas small amount of γ_1' variant is also formed with parallel plates structures. Formation of γ_1' phase is inevitable when the concentration of Al is more than 14.2% in the alloy irrespective of the other conditions and factors. Increase in the percentage concentration of Al increases the stability of γ_1'phases.

These phases are less ductile than β_1'phases. But here in this study Al concentration is less than aforementioned concentration percentage and hence the formation of β_1' phase is promoted. Minor addition of other elements (like Ti in this paper) in the alloys tend to form some intermetallic compounds which depletes the percentage of Al in the matrix and therefore lead to the formation of β_1'phase and therefore overall the formation β_1' is promoted in these three alloys. In case of 2H variant of martensite, the sizes of plates are long and thickness of each plate varies in a step manner on the either side of plates along longest plate. All the plates of γ_1' martensite phases are oriented in one single direction in one bunch and in another direction in another bunch. On the other hand, β_1' phase is oriented in different direction all over the microstructure. There are two variants of β_1' phases which can be observed in the micrographs: One with broad plates of long size whereas other with fine plates with small sizes, although the thickness of plates is less compared to CANB1 and CANB2. These martensite phases can be observed with twin patterns with self accommodating structures. These β_1' phases are randomly oriented in the alloys.

In Figure 6 (a), it can be clearly observed that thickness and length of β1' martensite in CANT1, are very large as compared to other two alloys [Figure 6(c, e)], although the length and concentration of γ1' martensite are less as compared to other two alloys, i.e., CANT2 and CANT3 alloys. Thick variants of 18R martensite with long sizes are oriented in the single direction (from right to left in the upper portion of micrograph) and comprising more than 50% of the micrograph [Figure 6 (a)]. Precipitation of X-phase in less quantity, has not caused ample hindrance to the growth of these plates and they are not intercepted by any other variants of martensite, therefore have grown in long sizes.In fact, these long plates have hindered the growth of other martensite plates at lower portion of the micrograph. Intercepting plates play a dominating role in the hindrance of growth of other martensite plates as compared to other factors, as indicated by the microstructural study.

On increasing the concentration of titanium in the alloy CANT2 and CANT3, the thickness and length of β_1' phase martensite have decreased to large extent. Since increase in the concentration of titanium may have provided large number of nucleation sites for precipitation, therefore reduction in the size of grain and martensite phases may have happened. Concentration of thick and long plates have decreased and depleted to give rise tothin and small variants of martensite as can be observed in Figure 6 (c) and (e). These plates are randomly oriented in different directions and are intercepting each other. Parallel lamellar structure of γ_1' phase have grown in large sizes and more in concentration in CANT2 and CANT3 as compared to that of CANT1.

As seen in Figure 6 (b, d and f), addition of Ti has led to the precipitation of second phase in the microstructures of CANT1, CANT2 and CANT3 alloys respectively. These precipitations are regular as well as irregular in shapes and have different sizes. These are termed as X-phase precipitates and have cubic Heusler type superstructure ($L2_1$) with composition close to $(Cu,Ni)_2 TiAl$. [38, 39] In Figure 6 (b), it can be observed that precipitation of X-phase is very less as compared to other two alloys, that is, CANT2 and CANT3. These precipitates are distributed more or less uniformly around the alloy. Some of them are also present in cluster form.

In Figure 6 (d and f), X-phases distributions can be observed as some are clustered together whereas majority of them are distributed throughout the microstructures. There are two types of X-phases in the present micrographs: one with large sizes of few microns termed as X_L which have flower shaped structures whereas one with very small sizes termed as X_S which have spherical or irregular shapes. Both of these phases can be identified in Figure 6 (a ,c and e) which are which are further depicted in Figure 6 (b, d and f) with higher magnification. These phases are responsible for the grain refinement and inhibit the grain growth during annealing. X_L is presumed to be precipitated in β_1 region during solidification whereas X_S is precipitated during quenching. X_L has incoherent interface with the β phase whereas XS has semi-coherent interface with the β phase [38,40]. Here it can be noted that with increase in Ti content, the amount of X-phase precipitations hasalso increased. These X-phases are also confirmed in X ray diffraction studies in Ti added alloys only which has been discussed above in XRD study section.

Hardness

Vickers Hardness values of all quenched samples are shown in Figure 7. It can be observed that alloying of Ti and B has increased the hardness of the base alloy [CAN]. These alloying have refined the grain size and structure of the base alloy to the great extent.

According to Hall-Petch equation $\sigma_y = \sigma_0 + k_y / \sqrt{d}$
Where
σ_y =yield strength of the material
σ_0 and k_y = constants for a particular material
d = average grain diameter

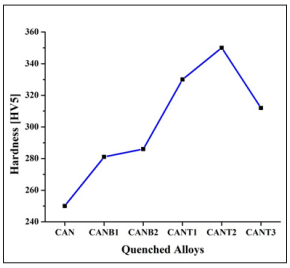

Figure 7: Vickers Hardness of Quenched Alloys

Yield strength of a material increases when average grain diameter decreases. Hence grain refinement increases the yield strength of the materials. The hardness of a material can be roughly taken to be proportional to the strength of the material [44,45].

Hardness α yield strength or Hardness $\alpha \frac{1}{(\sqrt{d})}(\sigma_y = \sigma_0 + k_y / \sqrt{d})$

Since the decrease in average grain diameter increases the yield strength of the materials; therefore, the increase in the strength results in increase in the hardness of the materials. Hence decrease in the grain size increases the hardness of the alloy which can be observed clearly in Figure 7. Increase in hardness of CANB1 and CANB2 alloy may be attributed to precipitation of boride particles which act as pinning agent for the motion of dislocation. In CANT1, CANT2 and CANT3, X-phase plays a significant role in controlling the grain growth rates at high temperature. The decrease in hardness of CANT3 may be attributed to dissolution of X-phase in the matrix of the alloy [16].

Conclusions

Transformation temperatures of all four alloys are above 373K which makes these alloys a potential alloys for high temperature applications. Distinct transformation peaks are obtained in all alloys other than CANB1 and CANT1. Boron addition resulted in increase in the transformation temperature of the alloys whereas the addition of titanium resulted in depression as compared to that of CAN alloy.

Micrographs of all the alloys in quenched state show the formation of martensite structures of different variants. Predominately 18R martensite with orthorhombic structures are formed in all the six alloys which are desirable for shape memory effect since they has self accommodating structures. Boron addition has led to the precipitation of second phase which are mainly aluminum boride particles or boron particles and also led to decrease in the length as well as thickness of β_1' martensite plates. Titanium addition led to the precipitation of second phase which is known as X-phase and also led to decrease in the thickness and length of β_1'martensite plates. These X-phase are of different shapes and sizes distribution.

XRD analysis confirms the presence of 18R martensite phase in all the six alloys and 2H martensite with parallel plates in case of all the alloys other than CANB1 and CANB2. Presence of X-phase is also confirmed by x-ray diffraction study in Ti added alloys.

Boron addition as well as titanium addition led to increase in the hardness of quenched alloys as compared to the base alloy CAN. Precipitation of second phase may be responsible for the increase in hardness in both the cases of boron addition as well as in the case of titanium addition.

Acknowledgment

The authors are highly thankful to CSIR New Delhi to fund this work under the CSIR-12th FYP in the area of 'development of thermo responsive high temperature SMAs. The authors are also thankful to the Director, CSIR-Advanced Materials and Processes Research Institute, Bhopal for providing facilities in laboratory to carry out the research works related to the paper. Mr. Shahadat Hussain is thankful to CSIR HRDG to provide fellowship to carry out his work.

References

1. K Otsuka, CM Wayman (1999) Shape memory materials, Cambridge university press.
2. F Butera, A Coda, G Vergani, SGetters SpA (2007) Shape memory actuators for automotive applications, Nanotec IT newsletter. Roma: AIRI/nanotec IT 12-16.
3. C Bil, K Massey, EJ Abdullah (2013) Wing morphing control with shape memory alloy actuators, Journal of Intelligent Material Systems and Structures 24: 879-898.
4. H Fujita, H Toshiyoshi (1998) Micro actuators and their applications, Microelectronics Journal 29: 637-640.
5. MM Kheirikhah, S Rabiee, ME Edalat (2010) A review of shape memory alloy actuators in robotics,Robot Soccer World Cup, Springer 206-217.
6. L Petrini, F Migliavacca (2011) Biomedical applications of shape memory alloys, Journal of Metallurgy.
7. TW Duerig, J Albrecht, GH Gessinger (1982) A shape-memory alloy for high-temperature applications, JOM 34: 14-20.
8. S Miyazaki, K Otsuka, H Sakamoto, K Shimizu (1981) The fracture of Cu–Al–Ni shape memory alloy, Transactions of the Japan institute of metals 22: 244-252.
9. MA Morris (1991) Influence of boron additions on ductility and microstructure of shape memory Cu9Al4 Ni alloys, Scripta metallurgica et materialia 25: 2541-2546.
10. R. Dasgupta (2014) A look into Cu-based shape memory alloys: Present scenario and future prospects, Journal of materials research 29: 1681-1698.
11. M Vollmer, C Segel, P Krooß, J Günther, L Tseng, et al. (2015) On the effect of gamma phase formation on the pseudoelastic performance of polycrystalline Fe–Mn–Al–Ni shape memory alloys, Scripta Materialia 108: 23-26.
12. S Bhattacharya, A Bhuniya, M Banerjee (1996) Influence of minor additions on characteristics of Cu–Al–Ni alloy, Materials science and technology 9: 654-658.
13. V Sampath (2005) Studies on the effect of grain refinement and thermal processing on shape memory characteristics of Cu–Al–Ni alloys, Smart materials and structures 14: S253.
14. S Vajpai, R Dube, S Sangal (2011) Microstructure and properties of Cu–Al–Ni shape memory alloy strips prepared via hot densification rolling of argon atomized powder preforms, Materials Science and Engineering A 529: 378-387.
15. S Miyazaki, T Kawai, K Otsuka (1982) On the origin of intergranular fracture in β phase shape memory alloys, Scripta metallurgica 16: 431-436.
16. G Sure, L Brown (1984) The mechanical properties of grain refined β-Cu-Al-Ni strain-memory alloys, Metallurgical and Materials Transactions A 15: 1613-1621.
17. K Enami (1982) Reordering and a New Ordered Phase in Ni-Al Martensite after Ageing, Le Journal de Physique Colloques 43: C4-727-C724-732.
18. Y Hanatate, M Miyagi, T Hamada, F Uratani (1982) The Effects of Boron on Grain Refinernent in Cu-AI-Ni Alloys, Report of Osaka industrial Technical Research Institute.
19. AH Kasberg, DJ Mack (1951) Isothermal Transformation And Properties Of A Commercial Aluminum Bronz, AIME TRANS 191: 903-908.
20. J Dennison, E Tull (1953) The Application Of Grain Refinement To Cast Copper-Aluminium Alloys Containing The Beta Phase, J. Inst. Metals 81.
21. R Elst, J Van Humbeeck, L Delaey (1985) Grain-growth in beta-copper-alloys, Zeitschrift fur metallkunde 76: 704-708.
22. K Enami, N Takimoto, S Nenno (1982) Effect of the Vanadium Addition on the Grain Size and Mechanical Properties of the Copper-Aluminium-Zinc Shape Memory Alloys, Le Journal de Physique Colloques 43: C4-773-C774-778.
23. M Miki, Y Ogino, Y Hiramatsu (1987) Effects of Boron and Chromium Additions on the Grain Refinement and Ductility of a Cu--14 Al--3 Ni Shape Memory Alloy, J. Jpn. Inst. Met 51: 815-823.
24. M Konishi, H Ohkuma, K Matsumoto, T Tsuno, H Kamei, et al. (1989) A novel antibiotic with the anthraquinone and 1, 5-diyn-3-ene subunit, The Journal of antibiotics 42: 1449-1452.
25. SN Saud, E Hamzah, T Abubakar, M Zamri, M Tanemura (2014) Influence of Ti additions on the martensitic phase transformation and mechanical properties of Cu–Al–Ni shape memory alloys, Journal of Thermal Analysis and Calorimetry, 118: 111-122.
26. M Zare, M Ketabchi (2017) Effect of chromium element on transformation, mechanical and corrosion behavior of thermomechanically induced Cu–Al–Ni shape-memory alloys, Journal of Thermal Analysis and Calorimetry 127: 2113-2123.
27. APandey, AKJain, S Hussain, V Sampath, R Dasgupta (2016) Effect of Nano CeO2 Addition on the Microstructure and Properties of a Cu-Al-Ni Shape Memory Alloy, Metallurgical and Materials Transactions B 47: 2205-2210.
28. X Zhang, J Sui, Q Liu, W Cai (2016) Effects of Gd addition on the microstructure, mechanical properties and shape memory effect of polycrystalline Cu-Al-Ni shape memory alloy, Materials Letters 180: 223-227.
29. MH Wu (1990) Copper-Based Shape Memory Alloys, Butterworth-Heinemann, Engineering Aspects of Shape Memory Alloys(UK) 69-88.
30. S Miyazaki, K Otsuka (1989) Development of shape memory alloys, Isij International 29: 353-377.
31. S Miyazaki (1996) Development and characterization of shape memory alloys, Shape Memory Alloys, Springer 69-147.
32. J Malimanek, N Zarubova (1995) Calommetric investigation of the movement of phase interfaces in a Cu-Al-Ni single crystal, Scripta metallurgica et materialia 32: 1347-1352.
33. A Prince, KH Kumar (1991) Aluminium–copper–nickel, Ternary alloys 4: 597-629.
34. S Stanciu, LG Bujoreanu, I Ioniţă, AV Sandu, A Enache (2009) A structural-morphological study of a Cu-63Al-26Mn11 shape memory alloy,Advanced Topics in Optoelectronics, Microelectronics, and Nanotechnologies IV, International Society for Optics and Photonics 72970C.
35. J Van Humbeeck, L Delaey, E Hornbogen, N Jost (1989) The Martensitic Transformation in Science and Technology, DGM, Oberursel 15-25.
36. K Sugimoto, K Kamei, H Matsumoto, S Komatsu, K Akamatsu, et al. (1982) Grain-refinement and the related phenomena in quaternary Cu-Al-Ni-Ti shape memory alloys, Le Journal de Physique Colloques 43: C4-761-C764-766.
37. J Lee, C Wayman (1986) Grain refinement of a Cu–Al–Ni shape memory alloy by Ti and Zr additions, Transactions of the Japan institute of metals 27: 584-591.
38. K Adachi, Y Hamada, Y Tagawa (1987) Crystal structure of the X-phase in grain-refined Cu-Al-Ni-Ti shape memory alloys, Scripta metallurgica 21: 453-458.
39. Hurtado, PRatchev, J Van Humbeeck, L Delaey (1996) A fundamental study of the χ-phase precipitation in Cu-Al-Ni-Ti-(Mn) shape memory alloys, Acta materialia, 44: 3299-3306.
40. J Font, J Muntasell, J Pons, E Cesari (1997) Thermal cycling

effects in high temperature Cu–Al–Ni–Mn–B shape memory alloys, Journal of materials research, 12: 2288-2297.
41. M Morris (1992) High temperature properties of ductile Cu-Al-Ni shape memory alloys with boron additions, Acta metallurgica et materialia, 40: 1573-1586.
42. AC Kneissl, E Unterweger, G Lojen, I Anzel (2005) Microstructure and Properties of Shape Memory Alloys, Microscopy and Microanalysis 11: 1704.
43. C Segui, E Cesari (1995) Ordering and stabilization in quenched CuAlNiMnB alloys, Journal of materials science 30: 5770-5776.
44. B Bardes (1978) Metals Handbook: Properties and Selection: Irons and Steels, vol. 1, American Society for Metals, Park, OH.
45. JR Davis, P Allen, S Lampman, TB Zorc, SD Henry, JL Daquila, et al. (1990) Metals handbook: properties and selection: nonferrous alloys and special-purpose materials, ASM International.